Correlation between resource-generating capacities of quantum gates

Aparajita Bhattacharyya, Ahana Ghoshal, Ujjwal Sen Harish-Chandra Research Institute, HBNI, Chhatnag Road, Jhunsi, Allahabad 211 019, India

We analyze the optimal product basis for generating the maximum relative entropy of quantum coherence by an arbitrary gate on a two-qubit system. The optimal basis is not unique, and the high quantum coherence generating gates are also typically high entanglement generating ones and vice versa. However, the profile of the relative frequencies of Haar random unitaries generating different amounts of entanglement for a fixed amount of quantum coherence is different from the one in which the roles of entanglement and quantum coherence are reversed, although both follow the beta distribution.

I. INTRODUCTION

The characterisation of resource theory, within quantum information science and technology, was initiated with the theory of entanglement [1–4]. In general, a resource theory is constructed by putting certain natural "constraints" or restrictions on the set of all quantum mechanical operations to perform a specific job, and the restrictions are overcome by utilizing certain "resources". The naturality of the constraints of course depend on the accessible physical system and the job at hand. In entanglement theory and practice, the restriction is set by the constraint that the observers - generally assumed to be at distant locations - will be able to perform only local quantum operations and classical communication (LOCC) and the "resources" are the entangled states shared by the same observers. In this manner, entanglement becomes useful in several interesting phenomena and tasks like quantum teleportation [5–7], quantum cryptography [8–10] and quantum dense coding [11, 12]. Quantum coherence [13–16] (see also [17–19]) is also one of the principal resources in quantum phenomena and information tasks, and along with being the reason for the classic interference phenomena, it is also useful in jobs like in quantum-enhanced metrology (see e.g. [20–22]), quantum algorithms (see e.g. [23–27]), quantum state discrimination (see e.g. [28, 29]), etc. The set of allowed operations are now the so-called incoherent operations, and the resources are the quantum coherent states.

Quantifying the entanglement generated by quantum evolutions has been extensively studied in the literature (see e.g. [30–49]). In particular, the two-qubit unitaries that generate maximal entanglement from zero resource pure input states (i.e., two-qubit pure product states) were identified, among other things, in Ref. [31]. The effect of auxiliaries on the entanglement generating ability was considered in e.g. [31, 35, 41]. The case of mixed state inputs was considered in e.g. [32, 34]. Generation of maximal entanglement using global unitaries of arbitrary bipartite dimensions was considered in e.g. [43]. The relation of entanglement generating capacities of two-qubit unitary operators with their distinguishability was uncovered in [45]. In Ref. [46], they found two-qubit mixed states whose entanglement content cannot be increased by unitary transformations.

Similar to the path followed in entanglement theory, various aspects of the quantitative theory of quantum coherence have been uncovered [13–16]. In particular, different properties of the incoherent and coherencegenerating operations have been identified, and maximally coherent states have been analyzed. It is understood that there exists interconnections between the resource theories of entanglement and quantum coherence. In particular, given a global unitary operation on a bipartite system, an arbitrary unentangled input state does not generate entanglement, and defining quantum coherence with respect to a basis related to those states that fails to generate entanglement, leads to such an intuitive interconnection. We remember that while entanglement is basis-independent as long as we stick to local bases, quantum coherence is almost strictly basis-dependent. Interrelations between the two resource theories have been studied in e.g. [50–61]. There has also been studies on interrelations between quantum coherence and other resources like "non-locality" [62–64], non-markovianity [65–70] and quantum discord [71–73]. Also, a relationship between classical communicationand entanglement-generating capacities of two-qubit unitary operators was found in [74]. In [75], they begin by considering a thermal state and find the maximum amount of quantum coherence that can be generated when acted upon by a unitary operator. In [76], they have constructed a basis-independent measure of quantum coherence and shown that it is equivalent to quantum discord. A quantum coherence-generating power for quantum channels, when it acts on incoherent states, was defined in [77]. Quantum coherence-generating power of quantum dephasing processes was considered in [78]. Parallel to the concepts of distillable entanglement [79, 80] and entanglement cost [79, 81], "quantum coherence distillation" and "quantum coherence cost" were considered in [15].

In this paper, we begin by exploring the maximal quantum coherence generating capacity for an arbitrary twoqubit unitary operator. The parallel case for entanglement was considered in [31]. We provide a formal definition of the capacity, which involves a maximum over all product bases of the underlying tensor-product Hilbert space. The analysis of the maximal quantum coherence generation is separately done for the "nonlocal" unitaries and the general ones. [The definition of a "nonlocal" unitary is given in the succeeding section.] We then compare the quantum coherence generation with entanglement generation for two-qubit unitaries. We find in particular that there exists a general tendency of a randomly chosen unitary to produce high quantum coherence when the entanglement generation is high, and conversely to produce high entanglement when the quantum coherence generation is so. We analyze the relative frequency of a randomly generated unitary to have a certain entanglement and quantum coherence generating capacity (with finite precision). We find that the profiles of the relative frequencies for a fixed quantum coherence generating capacity and a fixed entanglement generating one are qualitatively similar and follow the beta distribution, but are quantitatively different.

The remainder of the paper is arranged as follows. The relevant information from previous literature is discussed in Sec. II. This includes the definition of entanglement generating capacity and its evaluation for two-qubit unitary gates. We also present here a formal definition of the quantum coherence generating capacity of unitary gates. In Sec. III, we present our results on quantum coherence generating capacities of two-qubit unitaries. The capacities for the so-called "nonlocal" unitaries are considered in Sec. III A, while the case of a general two-qubit unitary is taken up in Sec. IIIB. We compare the entanglement and quantum coherence generations of several paradigmatic two-qubit gates in Sec. IV. In Sec. V, we consider the same comparison for Haar uniformly generated twoqubit unitaries. We present the concluding remarks in Sec. VI.

II. PRELIMINARIES

We wish to deal with the resource-generating capacities of two-party unitaries, when the resource is either entanglement or quantum coherence. Let the two parties be Alice (A) and Bob (B), with the system they possess being defined on the Hilbert space, $\mathcal{H}_A \otimes \mathcal{H}_B$.

The amount of entanglement generated by applying an arbitrary unitary operator U_{AB} is given by

$$E_g(U_{AB}) = \max_{\varrho_{AB}} \left[E\left(U_{AB}\varrho_{AB}U_{AB}^{\dagger}\right) - E\left(\varrho_{AB}\right) \right], \quad (1)$$

where the maximization is over all states, ϱ_{AB} , on $\mathcal{H}_A \otimes \mathcal{H}_B$, and where E is a measure of entanglement for two-party quantum systems. One can also choose to consider the more general situation where the evolution acts on locally extended Hilbert spaces, and an additional optimization is performed over all such extensions. For pure bipartite states, the local von Neumann entropy is a good measure of the state's entanglement [82], so that

$$E(|\psi\rangle) = -\text{Tr}(\rho_A \log_2 \rho_A) = -\text{Tr}(\rho_B \log_2 \rho_B),$$
 (2)

where ρ_A is the partial trace of $|\psi\rangle\langle\psi|$ over the subsystem B and similarly for ρ_B .

In this paper, we restrict to pure input states and to input states having zero resource. Therefore, the input states are pure product states, so that

$$E_g(U) = \max_{|\psi\rangle\otimes|\phi\rangle} S\left(\operatorname{Tr}_{A/B} P\left[U_{AB}|\psi\rangle_A \otimes |\phi\rangle_B\right]\right), \quad (3)$$

where $P[|\chi\rangle] = |\chi\rangle\langle\chi|$ and $S(\sigma) = -\text{Tr}(\sigma \log_2 \sigma)$. Moreover, we will restrict ourselves to two-qubit systems, for which the entanglement-generating capacity was considered in Ref. [31].

We next move over to quantum coherence generation by the unitary operator, U_{AB} . To deal with this question, we first need to fix the basis with respect to which the quantum coherence is to be calculated. Let us suppose that this basis of $\mathcal{H}_A \otimes \mathcal{H}_B$ is

$$\mathcal{B} = |\psi_i\rangle_{i=1}^{d_A d_B},\tag{4}$$

where $d_A = \dim \mathcal{H}_A$ and likewise for d_B . The quantum coherence, with respect to a basis \mathcal{B} , generated by the unitary, U_{AB} , is given by

$$C_g(U_{AB}|\mathcal{B}) = \max_{\varrho_{AB}} \left[C\left(U_{AB} \varrho_{AB} U_{AB}^{\dagger} | \mathcal{B} \right) - C\left(\varrho_{AB} | \mathcal{B} \right) \right], \tag{5}$$

where again, like in the case of entanglement generation, the maximization is over all states, ϱ_{AB} on $\mathcal{H}_A \otimes \mathcal{H}_B$. And again, it is possible to consider the generating capacity by considering an additional optimization over all local extensions on Alice's and Bob's spaces. C is a measure of quantum coherence, and while several quantum coherence measures are known in the literature, we consider the relative entropy of quantum coherence [14] for our purposes. Just like for the case of entanglement we will consider pure inputs, so that

$$C(|\psi\rangle|\mathcal{B}) = S(\rho_{diag}),$$
 (6)

where ρ_{diag} is a diagonal density matrix constructed by the diagonal elements of $|\psi\rangle\langle\psi|$, when written in the basis, \mathcal{B} . We focus only on product orthonormal bases of the bipartite system, for computing the relative entropy of quantum coherence. Arbitrary product bases in general bipartite quantum systems is a relatively less understood concept. However, for two-qubit systems, all product orthonormal bases have been characterized [83], and they can be expressed as

$$|0\eta\rangle, |0\eta^{\perp}\rangle, |1\eta\rangle, |1\eta^{\perp}\rangle.$$
 (7)

In the computational basis, the $|\eta\rangle$ and $|\eta^{\perp}\rangle$ can be written as $|\eta\rangle = \cos(\theta/2)|0\rangle + e^{i\phi}\sin(\theta/2)|1\rangle$ and $|\eta^{\perp}\rangle = -e^{-i\phi}\sin(\theta/2)|0\rangle + \cos(\theta/2)|1\rangle$.

Just like for the case of entanglement generation, we consider only those inputs for which the resource is vanishing. As we have already mentioned, we only consider pure inputs. Therefore, for quantum coherence generation with respect to a product orthogonal basis, $\mathcal{B}_{\mathbb{C}^2 \otimes \mathbb{C}^2}$,

on the two-qubit Hilbert space, the inputs can only be the four states of $\mathcal{B}_{\mathbb{C}^2\otimes\mathbb{C}^2}$. So finally, the amount of quantum coherence with respect to the basis, $\mathcal{B}_{\mathbb{C}^2\otimes\mathbb{C}^2}$, that is generated by using the unitary, U_{AB} , is given by

$$C_g(U|\mathcal{B}_{\mathbb{C}^2\otimes\mathbb{C}^2}) = \max_i C(U_{AB}|\phi_i\rangle_{AB}|\mathcal{B}_{\mathbb{C}^2\otimes\mathbb{C}^2}), \qquad (8)$$

where $\mathcal{B}_{\mathbb{C}^2 \otimes \mathbb{C}^2} = \{ |\phi_i\rangle_{AB} \}_{i=1}^4$. Now for obtaining the quantum coherence generating capacity of the unitary, we have to take a maximization over arbitrary product bases of the $\mathbb{C}^2 \otimes \mathbb{C}^2$ Hilbert space. So, we have

$$C_g(U) = \max_{\text{product bases } \mathcal{B}_{\mathbb{C}^2 \otimes \mathbb{C}^2}} \max_i C(U_{AB} | \phi_i \rangle_{AB} | \mathcal{B}_{\mathbb{C}^2 \otimes \mathbb{C}^2})$$
(9)

An arbitrary two-qubit unitary operator can be written in the form $[31,\,84]$

$$U_{AB} = U_A \otimes U_B U_d V_A \otimes V_B, \tag{10}$$

where $U_A, V_A, U_B, V_B \in U(2)$. U_A, U_B, V_A, V_B are unitaries acting on the local subsystems, and U_d is a "non-local" unitary on $\mathbb{C}^2 \otimes \mathbb{C}^2$ having the form,

$$U_d = \exp(-i\alpha_x \sigma_x \otimes \sigma_x - i\alpha_y \sigma_y \otimes \sigma_y - i\alpha_z \sigma_z \otimes \sigma_z), (11)$$

where α_x , α_y , α_z are real numbers and σ_x , σ_y , σ_z are the Pauli matrices. The relevant ranges for α_x , α_y , α_z may depend on the resource being generated, as we see below.

For obtaining the maximum entanglement generated by a fixed unitary, we have to perform a maximization over input states. Since we are taking the input states as arbitrary pure product states, we can forget about the V_A and V_B , because they will just rotate the space of product states into itself. Also, it is of no use, in this case, to apply the $U_A \otimes U_B$, as local unitaries will keep the entanglement unchanged. So, while generating entanglement by a two-qubit unitary, it is enough to only deal with U_d , as the amount of entanglement generated will not be affected by the four local unitaries. In Ref. [31], it was shown that whenever $\alpha_x + \alpha_y \ge \pi/4$ and $\alpha_y + \alpha_z \le \pi/4$, there always exists an input state for which we get maximal entanglement at the output, and outside the region - dictated by the above inequalities - in the $(\alpha_x, \alpha_y, \alpha_z)$ parameter space, the maximum entanglement is given by

$$E = H\left(\frac{1 + \sqrt{1 - \overline{C}^2}}{2}\right),\tag{12}$$

where $H(\cdot)$ is the binary entropy function, with \overline{C} being given by [85, 86]

$$\overline{C} = \max_{k,l} |\sin(\lambda_k - \lambda_l)|, \tag{13}$$

where k, l go from 1 to 4 and

$$\lambda_{1} = \alpha_{x} - \alpha_{y} + \alpha_{z},$$

$$\lambda_{2} = -\alpha_{x} + \alpha_{y} + \alpha_{z},$$

$$\lambda_{3} = -\alpha_{x} - \alpha_{y} - \alpha_{z},$$

$$\lambda_{4} = \alpha_{x} + \alpha_{y} - \alpha_{z}.$$
(14)

It is enough to consider the parameter range $\pi/4 \ge \alpha_x \ge \alpha_y \ge \alpha_z \ge 0$, as the maximal entanglement generated is a periodic function in the $(\alpha_x, \alpha_y, \alpha_z)$ parameter space, and completes a full period in this range.

Moving over to the case of maximal quantum coherence generation over product bases and with the unitary U_{AB} , we note that the product basis $\{|\phi_i\rangle\}_i$ in Eq. (8) is taken to another product basis by $V_A \otimes V_B$, which will anyway be considered in the maximization over product bases in (9). So, in (9), we can ignore the $V_A \otimes V_B$. $U_A \otimes U_B$ remains relevant throughout the quantum coherence part of this paper, and of course U_d is relevant in both entanglement and quantum coherence parts. For the optimizations, we have used the algorithms of NLOPT [87].

III. QUANTUM COHERENCE GENERATING CAPACITY OF UNITARY GATE

In this section, we try to find the maximum quantum coherence generating capacities of two-qubit unitary operators. We do this for two cases, of which the first is a particular case of the second. The second case is the general two-qubit unitary operator.

A. Special case: the nonlocal unitary U_d

We begin with the case where the local unitaries U_A , U_B , V_A and V_B are identity operators. So, we are left with only the nonlocal unitary, U_d , expressed in Eq. (11), and if we write it in matrix form in the computational basis, it looks like

$$U_d = \begin{pmatrix} \beta_1 & 0 & 0 & \beta_2 \\ 0 & \beta_3 & \beta_4 & 0 \\ 0 & \beta_4 & \beta_3 & 0 \\ \beta_2 & 0 & 0 & \beta_1 \end{pmatrix}, \tag{15}$$

where

$$\beta_{1} = e^{-i\alpha_{z}} \cos(\alpha_{x} - \alpha_{y}),$$

$$\beta_{2} = -ie^{-i\alpha_{z}} \sin(\alpha_{x} - \alpha_{y}),$$

$$\beta_{3} = e^{i\alpha_{z}} \cos(\alpha_{x} + \alpha_{y}),$$

$$\beta_{4} = -ie^{i\alpha_{z}} \sin(\alpha_{x} + \alpha_{y}).$$
(16)

For a fixed U_d , i.e., for a fixed set of values for α_x , α_y , α_z , we have to maximize the quantum coherence generated over all θ and ϕ , where the latter are parameters of the product basis, given in Eq. (7), with respect to which the quantum coherence is considered. For a given θ and ϕ , there are four inputs to be considered, and for each input, we obtain a quantum coherence of the output, which is a function of θ and ϕ . The maximal quantum coherence generated for U_d is the maximum of these four functions, each having been maximized over θ and ϕ , for every point in the $(\alpha_x, \alpha_y, \alpha_z)$ -space.

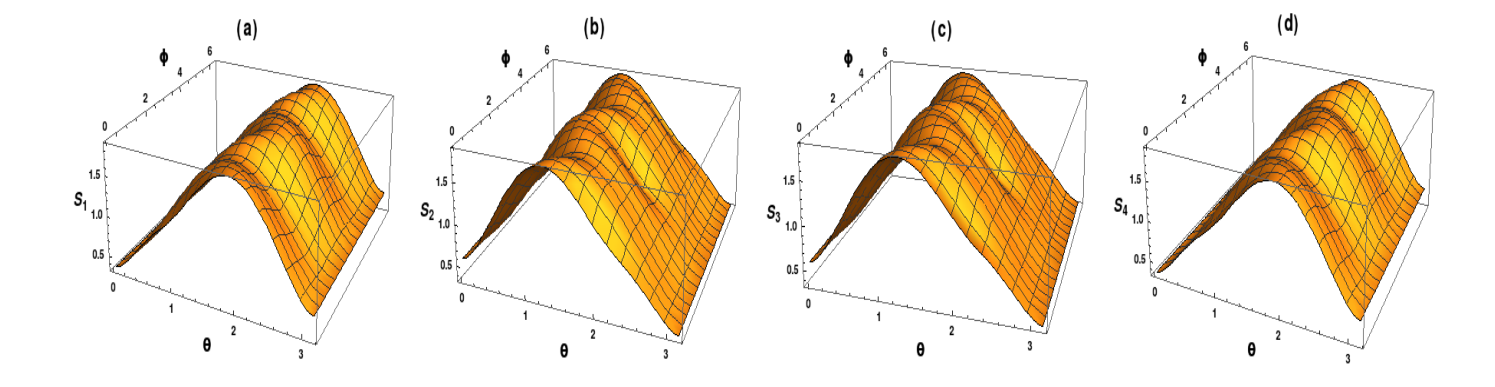


FIG. 1. Quantum coherence generation. We plot here the relative entropy of quantum coherence obtained from a given nonlocal unitary, U_d , with respect to the parameter space of input states. The four plots correspond to the four expressions of quantum coherence, S_1 , S_2 , S_3 and S_4 as functions of the input state parameters θ and ϕ , in panels (a), (b), (c) and (d) respectively. We have chosen $\alpha_x = 0.7231$, $\alpha_y = 0.4672$ and $\alpha_z = 0.1421$, for the plots. The θ and ϕ axes are in radians, and the vertical axis represents the generated relative entropy of quantum coherence (in bits).

Corresponding to the input states $|0\eta\rangle$, $|0\eta^{\perp}\rangle$, $|1\eta\rangle$ and $|1\eta^{\perp}\rangle$, the relative entropy of quantum coherence of the output states are respectively

$$S_i = -\sum_{l=1}^{2} \left[\gamma_{l_i} \log_2(\gamma_{l_i}) + \delta_{l_i} \log_2(\delta_{l_i}) \right], \qquad (17)$$

for i = 1, 2, 3, 4, where

$$\begin{split} \gamma_{l_1} &= |\beta_l|^2 \cos^4 \frac{\theta}{2} + |\beta_{l+2}|^2 \sin^4 \frac{\theta}{2} - \frac{1}{2} (-1)^l \Re \big(\xi_1 \big) \sin^2 \theta, \\ \gamma_{l_2} &= \left[|\beta_l|^2 + |\beta_{l+2}|^2 + \frac{1}{2} (-1)^l \Re \big(\xi_1 \big) \right] \sin^2 \theta, \\ \delta_{l_2} &= |\beta_l|^2 \sin^4 \frac{\theta}{2} + |\beta_{l+2}|^2 \cos^4 \frac{\theta}{2} - \frac{1}{2} (-1)^l \Re \big(\xi_1 \big) \sin^2 \theta, \\ \delta_{l_3} &= |\beta_l|^2 \sin^4 \frac{\theta}{2} + |\beta_{l+2}|^2 \cos^4 \frac{\theta}{2} - \frac{1}{2} (-1)^l \Re \big(\xi_2 \big) \sin^2 \theta. \\ \gamma_{l_3} &= \left[|\beta_l|^2 + |\beta_{l+2}|^2 + \frac{1}{2} (-1)^l \Re \big(\xi_2 \big) \right] \sin^2 \theta, \\ \gamma_{l_4} &= |\beta_l|^2 \cos^4 \frac{\theta}{2} + |\beta_{l+2}|^2 \sin^4 \frac{\theta}{2} - \frac{1}{2} (-1)^l \Re \big(\xi_2 \big) \sin^2 \theta, \end{split}$$

and $\delta_{l_1} = \gamma_{l_2}$, $\delta_{l_4} = \gamma_{l_3}$. Here we have used the notations, $\xi_1 = \beta_l^* \beta_{l+2} e^{2i(l-1)\phi}$ and $\xi_2 = \beta_l \beta_{l+2}^* e^{2i(l-1)\phi}$. Hence, following Eq. (8), the maximum quantum coherence for the fixed unitary and for the fixed basis is $\max\{S_1, S_2, S_3, S_4\}$, where the four S_i are given in Eq. (17). So, in accordance with Eq. (9), the maximum relative entropy of quantum coherence generated by the fixed unitary, U_d , is given by

$$C_g(U_d) = \max_{\theta, \phi} [\max\{S_1, S_2, S_3, S_4\}]$$
 (18)

All the four functions S_i are periodic with respect to each of α_x , α_y and α_z with a period of π . So, for evaluating the

generation of relative entropy of quantum coherence we can use the bounds, $\pi \geq \alpha_x, \alpha_y, \alpha_z \geq 0$, because beyond this region, the functions repeat their natures. Therefore for further illustration and analysis of the results, for the special case when the unitary is U_d , we have taken $\pi \geq \alpha_x \geq \alpha_y \geq \alpha_z \geq 0$.

1. A few numerical observations

Here we make some numerical observations regarding the quantum coherence generating capacity of a typical unitary among the nonlocal unitaries. We have observed that the four basis elements, when taken as input states, give the same value of maximal quantum coherence for any fixed set values of α_x , α_y and α_z , i.e., for a given U_d . Also, for a fixed unitary, the values of θ corresponding to the maximum quantum coherence are equal for the input states $|0\eta\rangle$ and $|1\eta^{\perp}\rangle$ in case of S_1 and S_4 , and for the input states $|1\eta\rangle$ and $|0\eta^{\perp}\rangle$ in case of S_2 and S_3 . This can be seen, e.g., in Fig. 1, where we have depicted S_1 , S_2 , S_3 and S_4 as functions of θ and ϕ , for a fixed unitary. From the figure, we can also see that the functions have a periodic nature with respect to ϕ . For a given basis state as input and for a given U_d , if we fix the value of θ at the point where any of the functions give its maximum, and look at the variation of quantum coherence with ϕ , we notice that the choice of ϕ for maximum quantum coherence is not unique. Within the range of 0 to 2π , there are four maxima in ϕ and the function is periodic with periodicity π . Also, the two functions of ϕ corresponding to the two basis states, $|0\eta\rangle$ and $|1\eta^{\perp}\rangle$, as inputs, are identical but with a certain shift, Δ , in ϕ . See Fig. 2. Similarly,

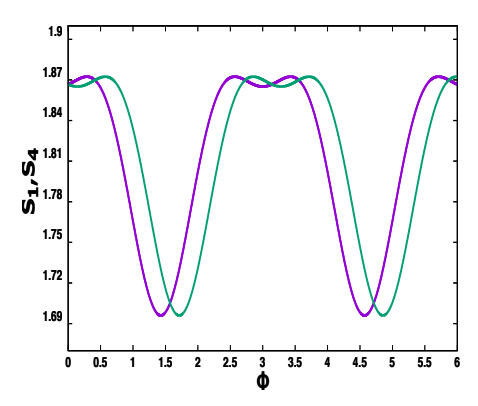


FIG. 2. Phase difference among the different quantum coherence generations for the different input states. We plot here the relative entropy of quantum coherence with respect to ϕ for a fixed θ . The violet curve corresponds to S_1 and the green one is for S_4 . Here we have fixed θ at the value that corresponds to the maximum values of S_1 and S_4 , and it is given by $\theta \approx 1.845$ radians. The values of the parameters of the unitary, U_d , are the same as in Fig. 1. Please see text for further details. The horizontal axis is in radians, while the vertical one is in bits.

the functions for the two states, $|0\eta^{\perp}\rangle$ and $|1\eta\rangle$, as inputs, are also identical except for the same phase shift Δ . This Δ depends on the parameters of the unitary, U_d . We will discuss more about Δ in Sec. III A 2. So, we realize that the choice of basis for getting the maximum quantum coherence, for a fixed unitary, is not unique. We can have at least two θ 's, and correspondingly different ϕ 's, for a certain maximum quantum coherence. Now we try to find analytical expressions for the basis parameters corresponding to a best choice of basis which can give us the maximum relative entropy of quantum coherence for

a fixed unitary.

2. Best choice of basis

The best choice of basis to obtain the maximum relative entropy of quantum coherence corresponds to the values of θ and ϕ (= θ_m and ϕ_m respectively) at which one of the four quantities S_1 , S_2 , S_3 and S_4 reaches its maximum, and is greater than or equal to the maximal values of the other three quantities. Let us assume the θ values for which the four functions S_1 , S_2 , S_3 and S_4 attain their maximum values are θ_{m_1} , θ_{m_2} , θ_{m_3} and θ_{m_4} , and the corresponding ϕ values are ϕ_{m_1} , ϕ_{m_2} , ϕ_{m_3} and ϕ_{m_4} respectively, for a fixed unitary. As we discussed in Sec. III A 1, $\theta_{m_1} = \theta_{m_4}$ and $\theta_{m_2} = \theta_{m_3}$. Also, $\phi_{m_4} = \phi_{m_1} + \Delta$ and $\phi_{m_3} = \phi_{m_2} + \Delta$. (θ_m, ϕ_m) is one among of the four pairs, $(\theta_{m_i}, \phi_{m_i})$, for i = 1, 2, 3, 4. Numerical observations have revealed that the four functions, S_i , provide the same maximum, possibly at different θ , ϕ . So, it is enough to maximize one of the four functions for obtaining the maximum quantum coherence generated by U_d , but the best choice of basis can be different for the four functions. In order to find the best choice of the basis for S_1 , we need to solve the following two equations for θ_{m_1} and ϕ_{m_1} :

$$\left. \frac{\partial S_1}{\partial \theta} \right|_{(\theta_{m_1}, \phi_{m_1})} = 0, \tag{19}$$

$$\frac{\partial S_1}{\partial \theta}\Big|_{(\theta_{m_1}, \phi_{m_1})} = 0,$$

$$\frac{\partial S_1}{\partial \phi}\Big|_{(\theta_{m_1}, \phi_{m_1})} = 0.$$
(20)

This assumes that the relevant extremum is not reached only at the boundary. We will come back to this issue later. From Eqs. (19) and (20), we obtain

$$\frac{\partial \delta_{1_1}}{\partial \theta} \log_2 \frac{\delta_{1_1}}{\gamma_{1_1}} + \frac{\partial \delta_{2_1}}{\partial \theta} \log_2 \frac{\delta_{2_1}}{\gamma_{2_1}} + \sin \theta \left[f(\theta) \log_2(\gamma_{1_1}) + g(\theta) \log_2(\gamma_{2_1}) \right] = 0 \quad \text{at } (\theta_{m_1}, \phi_{m_1}), \tag{21}$$

$$\cos[2(\alpha_z + \phi_{m_1})] = \frac{\left[\sin^2(\alpha_x - \alpha_y)\cos^2\frac{\theta_{m_1}}{2} - \sin^2(\alpha_x + \alpha_y)\sin^2\frac{\theta_{m_1}}{2}\right]\cos\theta_{m_1}}{\sin^2\theta_{m_1}\sin(\alpha_x + \alpha_y)\sin(\alpha_x - \alpha_y)},\tag{22}$$

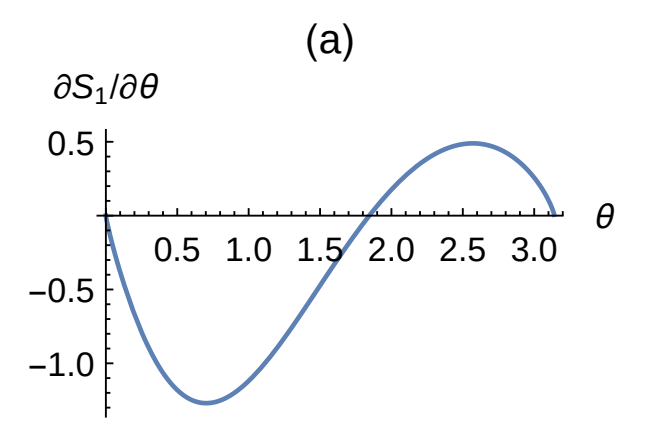
where
$$f(\theta) = -\cos^2(\alpha_x - \alpha_y)\cos^2\frac{\theta}{2} + \cos^2(\alpha_x + \alpha_y)\sin^2\frac{\theta}{2} + (\cos^2(\alpha_x - \alpha_y) + \cos^2(\alpha_x + \alpha_y))\frac{\cos\theta}{2},$$

$$g(\theta) = -\sin^2(\alpha_x - \alpha_y)\cos^2\frac{\theta}{2} + \sin^2(\alpha_x + \alpha_y)\sin^2\frac{\theta}{2} + (\sin^2(\alpha_x - \alpha_y) + \sin^2(\alpha_x + \alpha_y))\frac{\cos\theta}{2}.$$

Eq. (22) is a relation between θ_{m_1} and ϕ_{m_1} , for a fixed unitary, from which it is possible to easily get ϕ_{m_1} as a function of θ_{m_1} . So, by this substituting in Eq. (21), we will get an equation of a single variable, which we can solve for θ_{m_1} , and then putting this value of θ_{m_1} in Eq. (22), we can get the required value of ϕ_{m_1} . This $\theta_{m_1} = \theta_{m_4}$, and to find the corresponding ϕ value for S_4 , we have to find Δ . Let us try to calculate the shift

analytically from the expressions of relative entropy that we have obtained. Comparing the terms containing ϕ of Eq. (17) for i = 1 and 4, we get

$$2\Re(\beta_2^*\beta_4 e^{2i\phi}) = 2\Re(\beta_2 \beta_4^* e^{2i(\phi + \Delta)}). \tag{23}$$



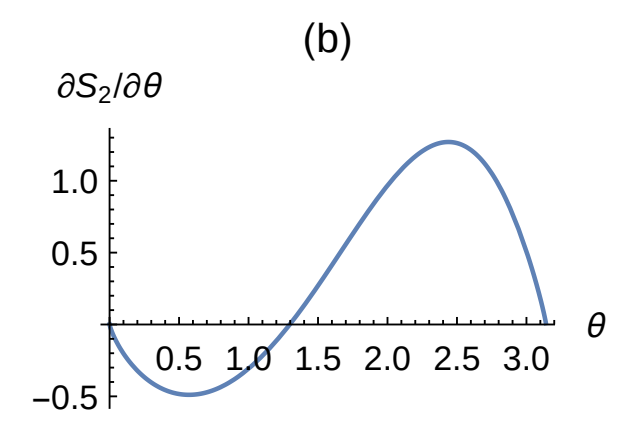


FIG. 3. In search of the best basis for quantum coherence generation. We plot here the function $\frac{\partial S_i}{\partial \theta}|_{(\theta_{m_i},\phi_{m_i})}$ after we have substituted ϕ_{m_i} in it as a function of θ_{m_i} using $\frac{\partial S_i}{\partial \phi}|_{(\theta_{m_i},\phi_{m_i})} = 0$. We have denoted θ_{m_i} as θ in the panels, for brevity. The plot in panel (a) is for i = 1, while that in panel (b) is for i = 2. The values of the parameters in the unitary U_d are the same as in Fig. 1. The horizontal axes are in radians and the vertical ones are in bits/radians.

If we substitute the values of β_2 and β_4 from Eq. (16), it follows that

$$\Delta = 2\alpha_z - n\pi,\tag{24}$$

where $n = 0, \pm 1, \pm 2, \dots$ Since we want the minimum shift, we consider n = 0. So, the shift depends on the

parameter, α_z , of the unitary, U_d . In particular, for the unitary that we have used in Figs. 1 and 2, we have $\Delta = 0.2842$. Hence, from the pair $(\theta_{m_1}, \phi_{m_1})$ for S_1 , we can find the set $(\theta_{m_4}, \phi_{m_4})$ for S_4 . Similarly for S_2 and S_3 , it is enough to find only one set of $(\theta_{m_i}, \phi_{m_i})$, for either i=2 or for i=3. The equations for optimizing S_2 for solving $(\theta_{m_2}, \phi_{m_2})$ are given by

$$\frac{\partial \gamma_{1_2}}{\partial \theta} \log_2 \frac{\gamma_{1_2}}{\delta_{1_2}} + \frac{\partial \gamma_{2_2}}{\partial \theta} \log_2 \frac{\gamma_{2_2}}{\delta_{2_2}} + \sin \theta \left[f_1(\theta) \log_2 \delta_{1_2} + g_1(\theta) \log_2 \delta_{2_2} \right] = 0 \quad \text{at } (\theta_{m_2}, \phi_{m_2}), \tag{25}$$

$$\cos[2(\alpha_z + \phi_{m_2})] = \frac{\left[\sin^2(\alpha_x + \alpha_y)\cos^2\frac{\theta_{m_2}}{2} - \sin^2(\alpha_x - \alpha_y)\sin^2\frac{\theta_{m_2}}{2}\right]\cos\theta_{m_2}}{\sin^2\theta_{m_2}\sin(\alpha_x + \alpha_y)\sin(\alpha_x - \alpha_y)},\tag{26}$$

where

$$f_1(\theta) = f(\theta) + \left[\cos^2(\alpha_x - \alpha_y) - \cos^2(\alpha_x + \alpha_y)\right],$$

$$g_1(\theta) = g(\theta) + \left[\sin^2(\alpha_x - \alpha_y) - \sin^2(\alpha_x + \alpha_y)\right].$$

The sets of $(\theta_{m_i}, \phi_{m_i})$ can be solved by various methods. We numerically solve for θ_{m_i} for a certain i, using the equation obtained from $\frac{\partial S_i}{\partial \theta}|_{\theta_{m_i}} = 0$ after substituting ϕ_{m_i} from $\frac{\partial S_i}{\partial \theta}|_{\phi_{m_i}} = 0$. See Fig. 3 for depictions of this equation in two cases. The functions corresponding to these equations have three zeros each, viz. at $0, \pi$ and at some intermediate point between 0 and π . The functions, S_i , attain their minimum values at 0 and π and reaches their maxima in between. So, the intermediate values are the ones that are relevant to us. For the U_d that we chose for the depictions in Figs 1 and $2, \theta_{m_1} \approx 1.845^c$ and $\theta_{m_2} \approx 1.297^c$, as exhibited in Fig. 3. And, $\theta_{m_4} = \theta_{m_1}$, $\theta_{m_3} = \theta_{m_2}$. But for all these four cases, the maximum relative entropy of quantum coherence generated by the

 U_d is the same, and is given by $C_g \approx 1.872$ bits. This fact is also seen in Fig. 1. The set of parameters of the unitary, which we have chosen for depiction in Figs. 1, 2 and 3, satisfy the conditions for generation of maximal entanglement [31].

3. Dependence of resource generating capacities on parameters of U_d

a. Highest quantum coherence generated by U_d that allows maximal entanglement generation. Next we find the maximum quantum coherence that can be generated by the unitary operators, U_d , which can maximize the entanglement of a bipartite quantum state to the maximal value, i.e., by those U_d for which $E_q(U_d) = 1$.

Kraus and Cirac [31] have shown that the maximal entanglement generated by a two-qubit unitary has certain periodicity and symmetry properties so that it is enough

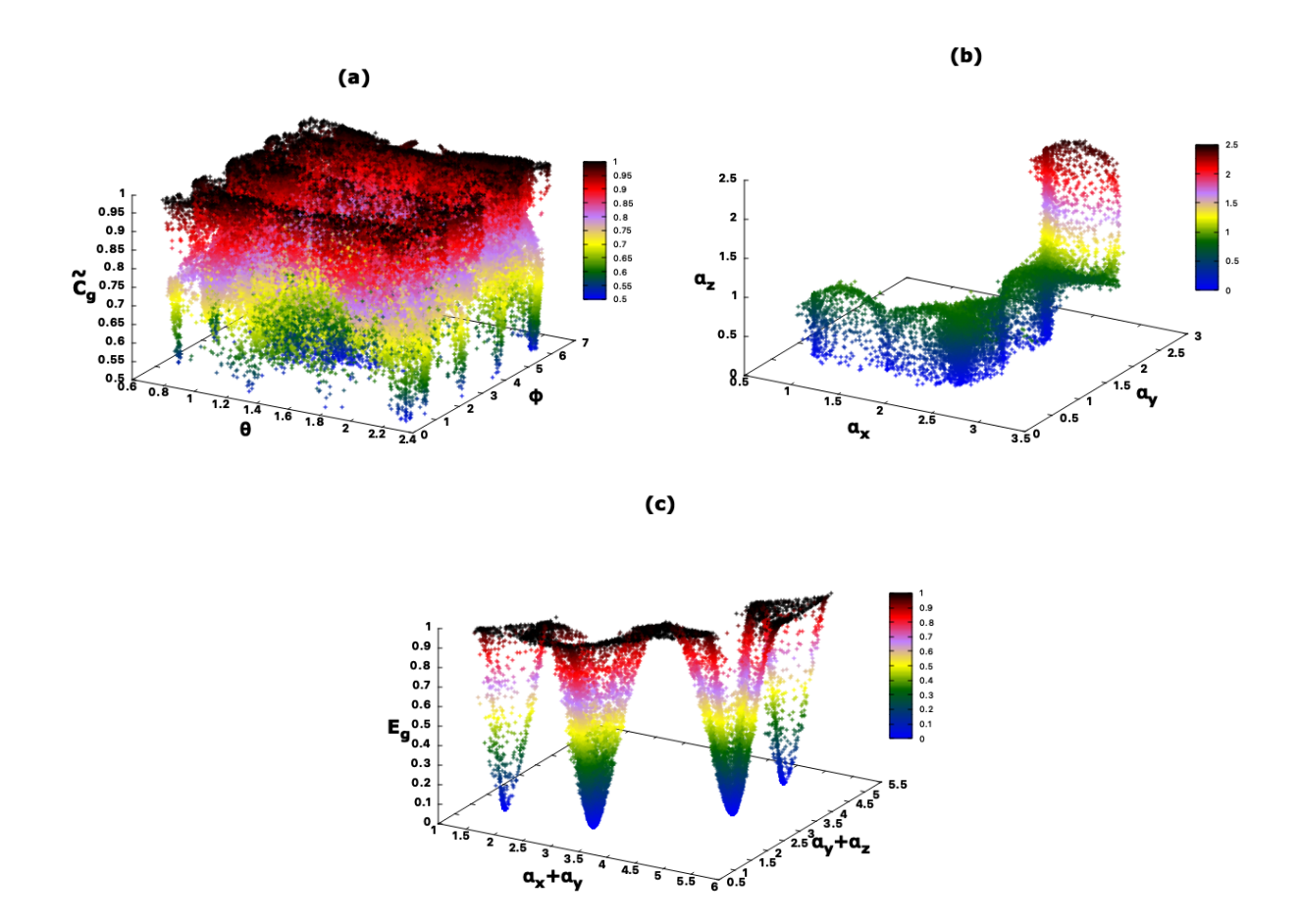


FIG. 4. Highest quantum coherence for maximal entanglement generating nonlocal unitaries, and vice versa. We investigate here the interplay between two resource generating capacities of the nonlocal unitaries, U_d . In panel (a), we generate 2×10^5 nonlocal unitaries which can create maximal entanglement, and plot the maximal relative entropy of quantum coherence that can be generated by the same. The plot is depicted against a base of (θ, ϕ) , the parameters of the optimal basis for the quantum coherence generation. The best choice of basis is not unique, and there always exist at least two θ_m 's in the whole range of 0 to π (see Fig. 1). The numerical optimization for the maximal quantum coherence has always picked the values of θ_m nearer to 0. Moreover, we are after finding the maximal quantum coherence generated, while a minimal one is generated at $\theta = 0$ and π . These explain the fact that we have not obtained the θ_m values in the full region of 0 to π , in panel (a). In panel (b), for 3.6×10^5 points, we mark the region of the parameter space of the nonlocal unitaries where the generated quantum coherence can reach the maximal value. In panel (c), the entanglement generating capacities of unitaries which can generate maximal quantum coherence are presented. For more details, please see the text. The θ , ϕ axes are measured in radians. α_x , α_y , α_z are dimensionless. The quantum coherence used in the plots are measured in bits, the entanglement therein are in ebits.

to consider the range $\pi/4 \geq \alpha_x \geq \alpha_y \geq \alpha_z \geq 0$. As previously discussed, the parameter region is bounded by 0 to π in case of evaluating the maximal quantum coherence generated, and this is the range that we use therefore for numerically or analytically analyzing quantum coherence generation or its interplay with entanglement generation. However, to keep using the expressions for entanglement generation from Ref. [31], we must identify the rule for going from the bigger range of parameters to the smaller one. This is as follows.

We choose the α_i , where i can be x or y or z, in the range $[0, \pi]$, and if we wish to find the maximal entanglement generated by the corresponding unitary, we set $\tilde{\alpha}_i = \alpha_i$ if $\alpha_i \leq \pi/4$ and $= \pi/2 - \alpha_i$ if $\pi/4 \leq \alpha_i \leq$

 $\pi/2$, and using the symmetry of generated entanglement around $\pi/4$, $U_d(\{\tilde{\alpha}_i\})$ and $U_d(\{\alpha_i\})$ generates the same entanglement. If $\alpha_i \in [\pi/2, \pi]$, we first use periodicity of the generated entanglement and go to an equivalent set of parameters α_i' - equivalent with respect to entanglement generation - where $\alpha_i' = \alpha_i - \pi/2$. If $\alpha_i' \in [0, \pi/4]$, then we set $\tilde{\alpha}_i = \alpha_i'$, and if $\alpha_i' \in [\pi/4, \pi/2]$, then we use the symmetry of the entanglement generated and set $\tilde{\alpha}_i = \pi/2 - \alpha_i'$.

So, now we have all the $\tilde{\alpha}_i$ in the parameter range 0 to $\pi/4$, but the order, $\alpha_x \geq \alpha_y \geq \alpha_z$, that was present in the range 0 to π , may get altered in case of the $\tilde{\alpha}_i$'s, as the symmetry about $\pi/4$ of generated entanglement is a reflection symmetry. Hence, the conditions $\alpha_x + \alpha_y \geq \pi/4$

and $\alpha_y + \alpha_z \leq \pi/4$ for obtaining maximal entanglement in case when the α_i belong to the range $[0,\pi/4]$, have to be modified. Suppose that after the mapping we have the order, $\tilde{\alpha}_i \geq \tilde{\alpha}_j \geq \tilde{\alpha}_k$, where i,j,k are from the set, $\{x,y,z\}$, and there are no repetitions. The conditions for getting maximal entanglement will then be $\tilde{\alpha}_i + \tilde{\alpha}_j \geq \pi/4$ and $\tilde{\alpha}_j + \tilde{\alpha}_k \leq \pi/4$. Therefore, we have the α_i 's in the parameter space 0 to π which can generate maximal entanglement. And now, we wish to analyze the maximal quantum coherence that can be generated by unitaries that can generate maximally entangled states.

In Fig. 4(a), we depict the maximum relative entropy of quantum coherence generated by the set of unitaries, U_d , which can generate maximal entanglement. The depiction is plotted against the optimal basis parameters for generating the maximal quantum coherence for that unitary. We generate 2×10^5 unitaries (U_d 's) for the plot. We notice that there are instances when a unitary generates both maximal entanglement and maximal quantum coherence. The maximum value of relative entropy of quantum coherence for a two-qubit system is 2 bits, but here, for easy comparison with the maximal value of generated entanglement, we normalise the generated quantum coherence as

$$\tilde{C}_q(U_d) = (1/2)C_q(U_d),$$
(27)

and so we get the maximum quantum coherence equal to 1 bit instead of 2 bits. We remember that the maximal value of generated entanglement in a two-qubit system, according to the definition that we have used, is 1 ebit.

- b. Maximal quantum coherence generating nonlocal unitaries. We now try to identify the α_x , α_y and α_z , corresponding to which we get $\tilde{C}_g(U_d)=1$, when we act the unitary operator U_d on an incoherent two-qubit pure quantum state. We depict this in Fig. 4(b), in the range $\pi \geq \alpha_x \geq \alpha_y \geq \alpha_z \geq 0$ by optimizing the relative entropy of quantum coherence of the output states.
- c. Highest entanglement generated by U_d that allows maximal quantum coherence generation. In Fig. 4(c), we look at the entanglement that can be generated by the unitaries which can generate maximum quantum coherence while operating on the set of two-qubit incoherent pure states. The unitaries are chosen from Fig. 4(b). We use the parameters $\alpha_x + \alpha_y$ and $\alpha_y + \alpha_z$ as axes of the base against which the generated entanglement is depicted. Note however that these α_x , α_y , α_z belong to the range $[0,\pi]$, and so for calculation of the maximal entanglement generation, we need to go to the range $[0, \pi/4]$, as in paragraph III A 3 a. And since there is a reflection symmetry that is used in the transformation between the two ranges, the ordering between the α 's is lost. Consequently, the condition for reaching maximal entanglement from Ref. [31] cannot be used directly in the presentation in panel (c). We have used 3.6×10^5 unitaries for the depiction. In Fig. 4(c), we find a finite probability of points (representing unitaries) for which the generated entanglement is 1 ebit. From panels (a) and (c) in the same figure, we can conclude that there

exists unitaries for which both entanglement and quantum coherence generations are maximal. The periodicity of $\pi/2$ and the symmetry about $\pi/4$ of entanglement in the parameter space lead to the periodicity of π and symmetry about $\pi/2$ of entanglement with respect to $\alpha_x + \alpha_y$ and $\alpha_y + \alpha_z$, and the latter are visible from the depiction (see panel (c) of Fig. 4).

B. The general two-qubit unitary

In this subsection, we attempt to find the maximum quantum coherence that an arbitrary two-qubit unitary operator can generate, but this time we keep the local parts, U_A , U_B , V_A and V_B . So the total unitary is of the form.

$$U_{AB} = U_A \otimes U_B U_d V_A \otimes V_B. \tag{28}$$

We set $W_1 = V_A$, $W_2 = V_B$, $W_3 = U_A$ and $W_4 = U_B$, with $W_k \in SU(2)$ for k = 1, 2, 3, 4, represented as

$$W_{k} = \begin{pmatrix} \cos\frac{\theta_{k}}{2}e^{\frac{i}{2}(\psi_{k} + \phi_{k})} & \sin\frac{\theta_{k}}{2}e^{-\frac{i}{2}(\psi_{k} - \phi_{k})} \\ -\sin\frac{\theta_{k}}{2}e^{\frac{i}{2}(\psi_{k} - \phi_{k})} & \cos\frac{\theta_{k}}{2}e^{-\frac{i}{2}(\psi_{k} + \phi_{k})} \end{pmatrix}. \quad (29)$$

where $\theta_k \in [0, \pi]$, $\phi_k \in [0, 2\pi]$ and $\psi_k \in [0, 4\pi)$. The form of the nonlocal unitary, U_d , remains the same as in Eq. (11). We choose an arbitrary product basis according to Eq. (7), and evaluate the expression for the relative entropy of quantum coherence which is generated by U_{AB} when acting on an incoherent pure two-qubit quantum state. The unitary U_{AB} of the form given in Eq. (28) can be expressed as

$$U_{AB} = \begin{pmatrix} r_3 & r_1 & m_3 & m_1 \\ r_7 & r_5 & m_7 & m_5 \\ r_4 & r_2 & m_4 & m_2 \\ r_8 & r_6 & m_8 & m_6 \end{pmatrix}.$$
(30)

Like for the nonlocal unitaries considered in the preceding section, we again calculate the relative entropy of quantum coherence for each of the states in the basis, $\{|0\eta\rangle, |0\eta^{\perp}\rangle, |1\eta\rangle, |1\eta^{\perp}\rangle\}$. They are respectively given by

$$\tilde{S}_i = -\sum_{l_i=1}^{2} \left[\tilde{\gamma}_{l_i} \log_2(\tilde{\gamma}_{l_i}) + \tilde{\delta}_{l_i} \log_2(\tilde{\delta}_{l_i}) \right], \quad (31)$$

for i=1,2,3,4, where the constituent quantities are given in Appendix A. The expressions for $\tilde{\gamma}_{l_3}$, $\tilde{\delta}_{l_3}$, $\tilde{\gamma}_{l_4}$ and $\tilde{\delta}_{l_4}$ for \tilde{S}_3 and \tilde{S}_4 are exactly same as $\tilde{\gamma}_{l_1}$, $\tilde{\delta}_{l_1}$, $\tilde{\gamma}_{l_2}$ and $\tilde{\delta}_{l_2}$ respectively, but only the r_j 's are replaced by m_j 's, where j runs from 1 to 8. If we fix the unitary, i.e., if we fix all r_j 's and m_j 's, we can maximise these four functions with respect to θ and ϕ - parameters of the product basis. In Fig. 5, we plot the four \tilde{S}_i 's with respect to the basis parameters for a fixed unitary. The numerical values of the parameters of the unitary considered here are given

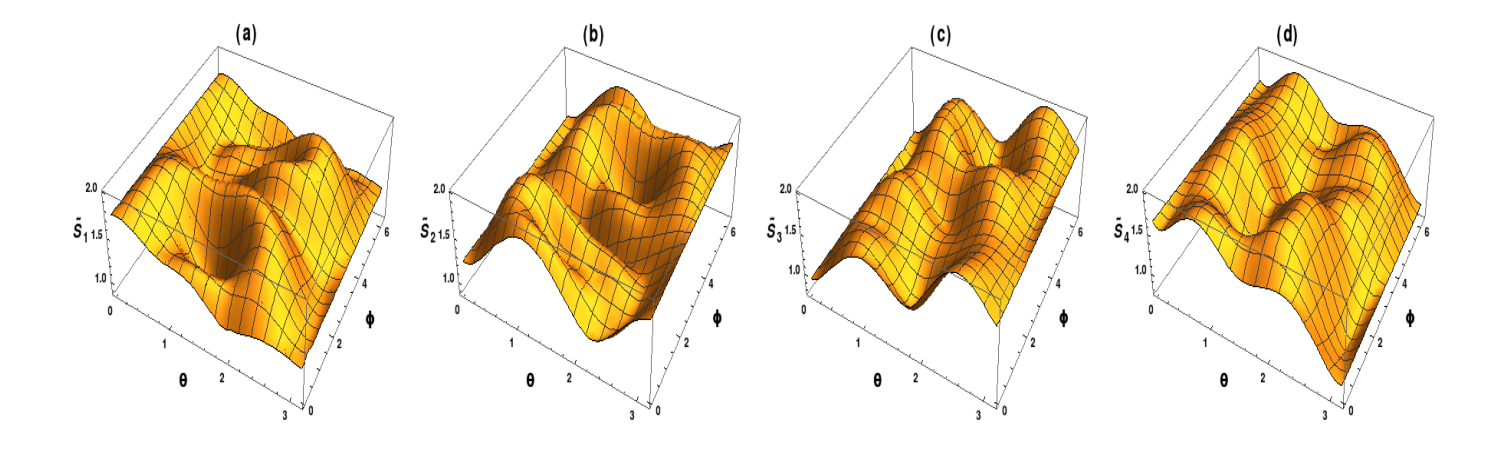


FIG. 5. Quantum coherence generation for a general two-qubit unitary. We plot here the relative entropy of quantum coherence that can be generated by the unitary, U_{AB} , as a function of the parameters of the product basis with respect to which the quantum coherence is defined and the elements of which act as initial states for the unitary evolution. The four plots are for the four elements of the product basis that act as the initial states of the evolution. The functions \tilde{S}_1 , \tilde{S}_2 , \tilde{S}_3 and \tilde{S}_4 are plotted with respect to the basis parameters, θ and ϕ , in panels (a), (b), (c) and (d) respectively. The fixed parameters of the unitary is taken as $\alpha_x = 0.6078$, $\alpha_y = 0.2625$, $\alpha_z = 0.2287$, $\theta_1 = 2.233$, $\phi_1 = 2.163$, $\psi_1 = 1.198$, $\theta_2 = 3.070$ $\phi_2 = 6.063$, $\psi_2 = 9.091$, $\theta_3 = 1.100$, $\phi_3 = 1.657$, $\psi_3 = 6.353$, $\theta_4 = 1.919$, $\phi_4 = 5.211$ and $\psi_4 = 11.26$. The quantities θ and ϕ in the horizontal axes are presented in radians and the vertical axes are in bits. The θ_i , ϕ_i and ψ_i , for i = 1, 2, 3, 4, are in radians.

in the caption of Fig. 5. The nature of the functions are quite different from our previous case, where instead of the full unitary U_{AB} , only the nonlocal unitary U_d was considered. In the previous case, each function had only one maximum with respect to θ in $[0,\pi]$, whereas in this case, there are several. Compare Figs. 1 and 5. This time it can be cumbersome to obtain the best choice of basis analytically, but it can be done numerically, using globally convergent routines. For a fixed unitary, we have observed numerically that the maximum quantum coherence corresponding to the initial states $|0\eta\rangle$ and $|0\eta^{\perp}\rangle$ (the maximum values of \tilde{S}_1 and \tilde{S}_2) are exactly equal. Similarly, for the states $|1\eta\rangle$ and $|1\eta^{\perp}\rangle$, the maximum values of \tilde{S}_3 and \tilde{S}_4 are also equal. But the pairs $(\tilde{S}_1, \tilde{S}_2)$ and $(\tilde{S}_3, \tilde{S}_4)$ do not have the same maximum values. This observation differs from the case in which only the nonlocal unitary (U_d) was used, as there, all four maxima were equal. We also observed in the the case of nonlocal unitary that although the ϕ_{m_i} values are not equal for different i, the θ_{m_i} values are the same for the functions S_i . This aspect is also missing here in the general unitary case. Here, along with possibility that the $\hat{\theta}_{m_i}$'s are different for different i, each of the functions, \tilde{S}_i , can have multiple maxima in the parameter space of θ in $[0,\pi]$. So, we have that for a general unitary, the best choice of basis for quantum coherence generation is not unique and the number of best bases can even be more than four. We have numerically observed that as in the case of the nonlocal unitary, the four functions, \hat{S}_i , are periodic in each of α_x , α_y and α_z , and considering the

parameter range $[0, \pi]$ for the α 's is sufficient, and we use this information for further analysis and illustration of the quantum coherence generating capacities of U_{AB} 's.

1. Dependence of resource generating capacities on parameters of U_{AB}

As in our previous search in Sec. III A 3 using nonlocal unitaries, we try to compare here between the same resource generating capacities (entanglement and quantum coherence), but now of the general unitary, U_{AB} . As mentioned earlier, the local unitaries V_A and V_B have no contribution in the maximal creation of entanglement and they also do not effect the maximum generated quantum coherence. So, here we do the analysis and illustration by discarding the $V_A \otimes V_B$ part and considering $\tilde{U}_{AB} = U_A \otimes U_B U_d$ as equivalent to the whole unitary U_{AB} .

a. Highest quantum coherence generated by U_{AB} that allows maximal entanglement generation. For this analysis, we first evaluate $\tilde{U}_{AB} |\psi\rangle_A \otimes |\phi\rangle_B$ for arbitrarily chosen parameters of the unitary, and then calculate the local von Neumann entropy of the output state and optimize over all $|\psi\rangle_A$, $|\phi\rangle_B \in \mathbb{C}^2$, where $|\psi\rangle_A$ and $|\phi\rangle_B$ are taken as

$$|\psi_A\rangle = \cos(\bar{\alpha}/2) |0_A\rangle + e^{i\bar{\beta}} \sin(\bar{\alpha}/2) |1_A\rangle, |\phi_B\rangle = \cos(\bar{\gamma}/2) |0_B\rangle + e^{i\bar{\delta}} \sin(\bar{\gamma}/2) |1_B\rangle.$$
(32)

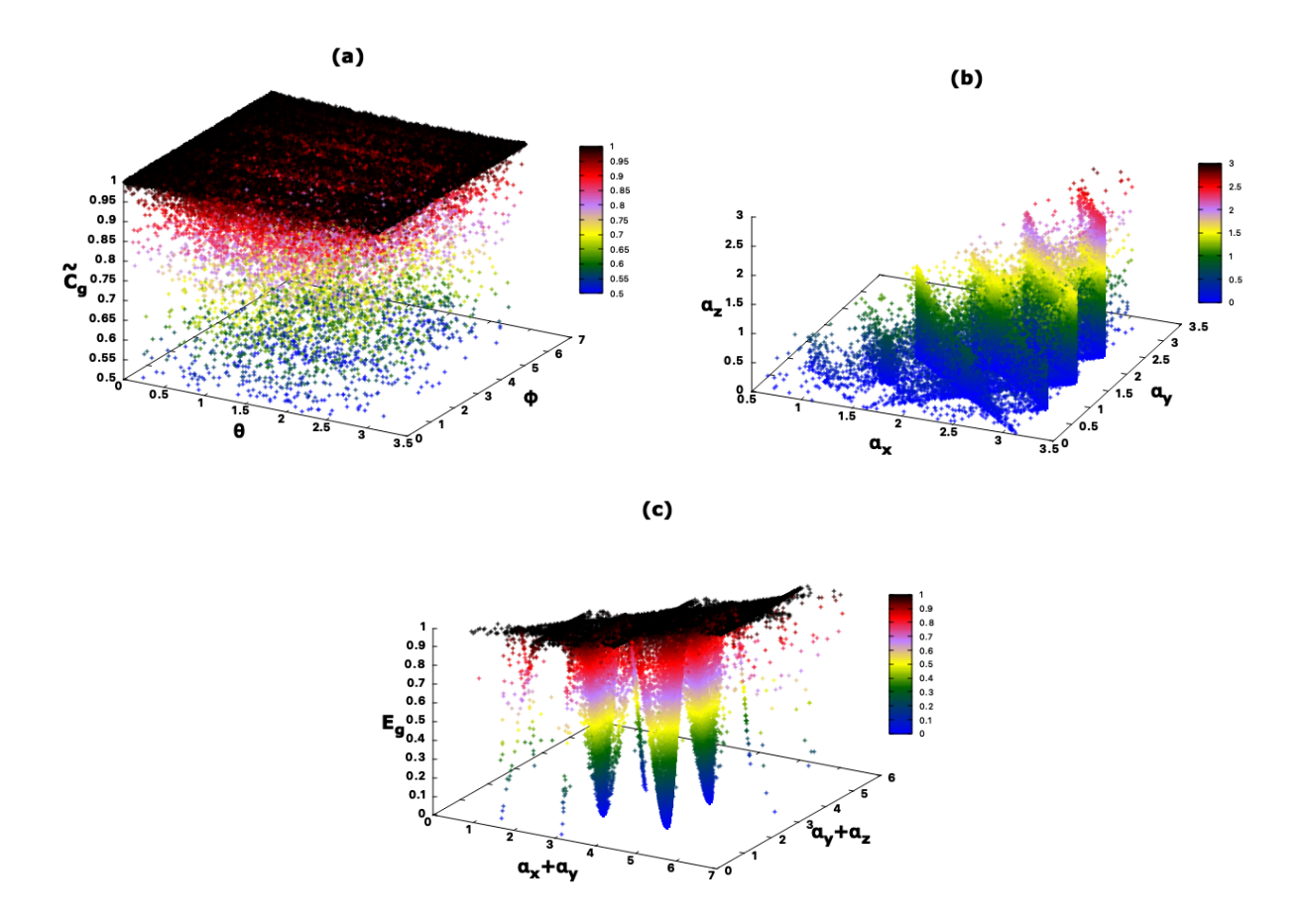


FIG. 6. Highest quantum coherence for maximal entanglement generating unitaries, and vice versa. The considerations here are exactly the same as in Fig. 4, except that general two-qubit unitaries are used here, instead of the nonlocal unitaries only. There are 1.3×10^5 unitaries used in panel (a), while there are 7.7×10^4 points in panel (b). Please see text for more details.

Therefore, to find the best entanglement generation, the maximization will be over $\bar{\alpha}, \bar{\gamma} \in [0, \pi]$ and $\bar{\beta}, \bar{\delta} \in [0, 2\pi)$, of $S(\operatorname{tr}_{A/B}P[\tilde{U}_{AB}|\psi\rangle_A\otimes|\phi\rangle_B])$, for every set of values of the parameters \tilde{U}_{AB} , which are α_x , α_y , α_z , θ_i , ϕ_i and ψ_i , where i stands for 3 and 4. We choose 5×10^6 unitaries in this parameter space, which can create maximal entanglement, and search for the maximum relative entropy of quantum coherence maximized over arbitrary pure product bases. The algorithm Direct-L [92] of NLOPT is used for the optimization. The analysis indicates that the probability for finding maximal quantum coherence is much larger now, in comparison to when the same analysis was performed for nonlocal unitaries, U_d . See Fig. 6(a). This is intuitively satisfactory as while local unitaries cannot create entanglement, they can create quantum coherence. It may be noted that instead of numerically optimizing entanglement with respect to the parameters of \tilde{U}_{AB} to identify the unitaries which can generate maximal entanglement, one can also decompose the unitary matrix into the form given in Eq. (28) following the procedure suggested in [31], and then the constraints on the parameters of the unitaries for generating $E_g(U_{AB}) = 1$ can be used, as we did in case of

 U_d 's.

b. Maximal quantum coherence generating unitaries. We now repeat the numerics (maximization using Isres [93]) that we used for identifying nonlocal unitaries that generate maximal quantum coherence, for general unitaries. The number of parameters for \tilde{U}_{AB} are greater than those in U_d . In Fig. 6(b), we try to identify the region of the $(\alpha_x, \alpha_y, \alpha_z)$ -space for random choice of the remaining parameters (i.e., θ_j , ϕ_j and ψ_j , for j running over 3 and 4), at which the unitary, \tilde{U}_{AB} , can lead to maximal quantum coherence.

c. Highest entanglement generated by U_{AB} that allows maximal quantum coherence generation. We now try to understand the amount of entanglement that can be generated by two-qubit unitaries that can give rise to maximal quantum coherence. We identify these unitaries from the considerations in Fig. 6(b). We map the α_i 's for those unitaries to those of the equivalent unitaries in the range $[0, \pi/4]$ - "equivalent" in terms of entanglement generation and the mapping is as discussed in Sec. III A 3. This exercise was performed for nonlocal unitaries in Fig. 4(c). The current case is depicted in Fig. 6(c). As in the previous case, the depiction of the

 E_g is against a base of $\alpha_x + \alpha_y$ and $\alpha_y + \alpha_z$. The periodicity and symmetry in the parameters for the function are not clearly visible in Fig. 6(c). This, we believe, is a result of the fact that the generation of unitaries in this section was with respect to the parameter space. The reason of this is that we wanted to compare the results obtained for arbitrary unitaries with those obtained for nonlocal unitaries, and the latter do not form a continuous group. The analysis in Sec. V, however, uses Haar uniform generation of unitaries.

IV. RESOURCE GENERATING CAPACITIES OF PARADIGMATIC QUANTUM GATES

We choose a few paradigmatic two-qubit gates that are widely used in quantum device circuits, and compare their entanglement and quantum coherence generating capacities. For completeness, we first define the gates, and then present a table containing the capacities.

Arguably, the most well-known two-qubit gate is the controlled-NOT (CNOT) operator. The NOT gate is the same as the Pauli- σ_x operator. The CNOT operator is defined on the two-qubit space as $U_{CNOT} = |0\rangle\langle 0|\otimes I_2+|1\rangle\rangle 1|\otimes\sigma_x$, where I_2 is the identity operator on the qubit space. The CNOT is therefore the controlled- σ_x operator. Similarly, one can consider the controlled- σ_z operator as $U_{CZ} = |0\rangle\langle 0|\otimes I_2+|1\rangle\rangle 1|\otimes\sigma_z$, which is usually referred to as the CZ gate. The SWAP is a two-qubit linear operator defined as $U_{SWAP}|\psi\rangle|\phi\rangle = |\phi\rangle|\psi\rangle$, where $|\psi\rangle, |\phi\rangle \in \mathbb{C}^2$. [One can of course define a swap gate in arbitrary bipartite dimensions, $\mathbb{C}^d\otimes\mathbb{C}^d$.] The SWAP of course cannot create any entanglement by acting on a product state. The situation is very different for its square root, for which the matrix representation in the computational basis, is

$$U_{\sqrt{SWAP}} = \begin{pmatrix} 1 & 0 & 0 & 0\\ 0 & \frac{1}{2}(1+i) & \frac{1}{2}(1-i) & 0\\ 0 & \frac{1}{2}(1-i) & \frac{1}{2}(1+i) & 0\\ 0 & 0 & 0 & 1 \end{pmatrix}.$$
(33)

So far, we have not considered any product unitary (i.e., product of two single-qubit unitaries), which trivially have vanishing entanglement generating capacities. They however can have nontrivial quantum coherence generating capacities. We consider three such product unitary gates. The first one that we choose is $U_{YX} = \sigma_y \otimes \sigma_x$. One can of course consider any other combination of the Pauli spin-1/2 operators. An important single-qubit unitary, that is almost universally present in a quantum algorithm circuit, is the Hadamard gate, defined by $H|0\rangle = \frac{1}{\sqrt{2}}(|0\rangle + |1\rangle)$, $H|1\rangle = \frac{1}{\sqrt{2}}(|0\rangle - |1\rangle)$, supplemented by linearity. The other two product unitaries that we consider are $H \otimes H$ and $H \otimes I_2$.

In the following table, we present the capacities of entanglement and quantum coherence generation for the above unitaries, correct to four significant figures.

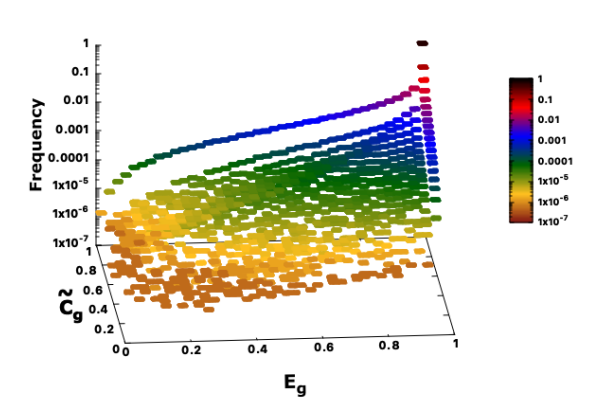


FIG. 7. Resource generating tendencies of Haar random twoqubit unitaries. We Haar uniformly generate a large number of two-qubit unitaries, and find their entanglement and quantum coherence generating capacities. We then divide the (E_g, \tilde{C}_g) space into small squares, and find the relative frequencies of the number of unitaries that fall in those squares. These relative frequencies are plotted along the vertical axis, which is on a logarithmic scale. The quantity plotted in the vertical axis is dimensionless, while the E_g and \tilde{C}_g are in ebits and bits respectively. Please see text for more details.

Gate (U)	$E_g(U)$	$\tilde{C}_g(U)$
CNOT	1	0.5
CZ	1	0.5
SWAP	0	1
$\sqrt{\text{SWAP}}$	1	0.8293
YX	0	0.5
$H \otimes H$	0	1
$H\otimes I_2$	0	0.5

In the succeeding section, we look at Haar uniformly generated random two-qubit unitaries, and compare their entanglement and quantum coherence generating capacities

V. RESOURCE GENERATING CAPACITIES OF HAAR RANDOM QUANTUM GATES

In this section, we will compare the entanglement and quantum coherence generating capacities of Haar uniformly generated gates on two-qubit systems. The Haar uniform generation is effected by using the Ginibre ensemble [88]. For each unitary, we numerically evaluate the E_g , by optimizing over arbitrary two-qubit pure product states as inputs (Eq. (32)). For the same unitary, we also obtain \tilde{C}_g for a pure incoherent input state, and optimize over the inputs as well as the product basis (Eq. (7)) with respect to which the quantum coherence is defined. The two maximizations are done independently, so that the input state for which the maximum entanglement is attained, can different from the state for which we

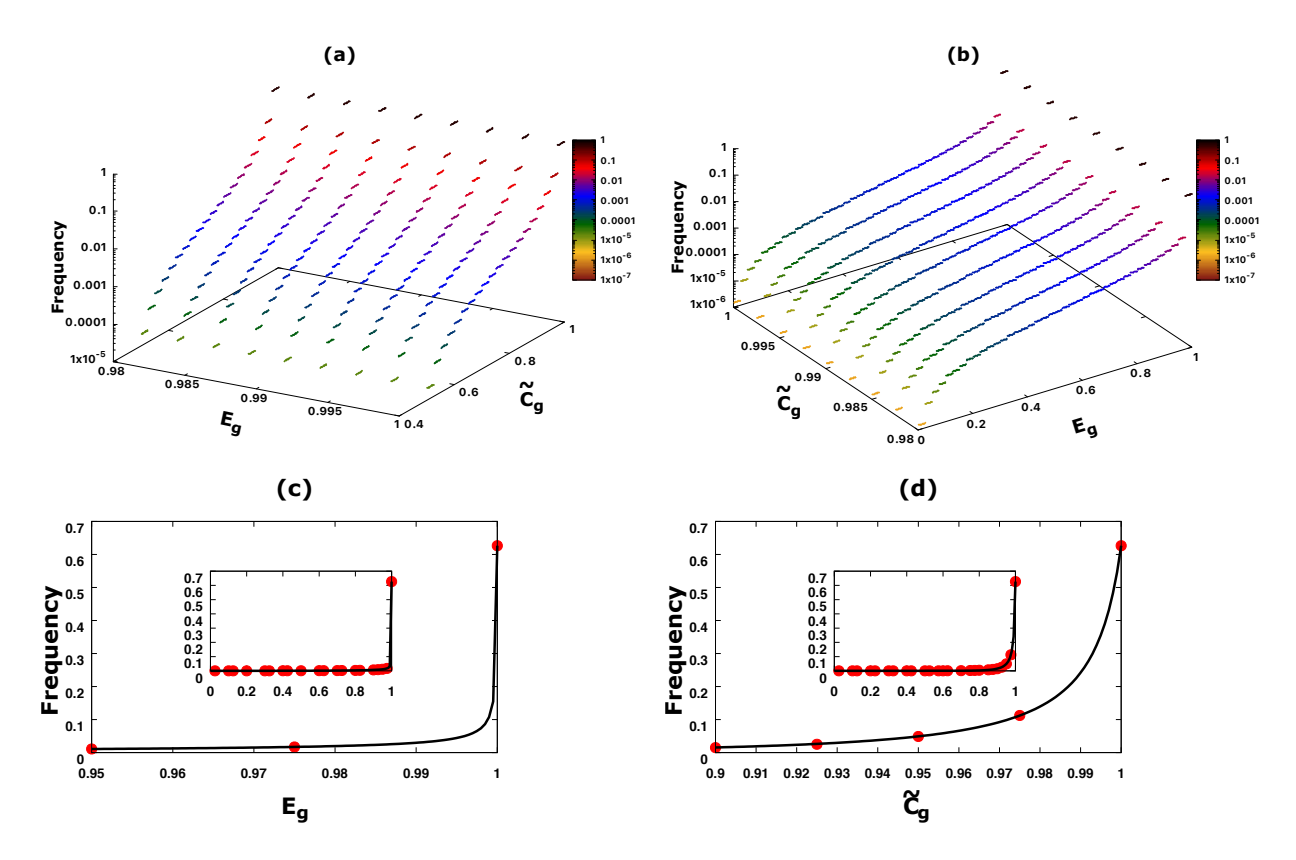


FIG. 8. The asymmetrical nature of resource generations of two-qubit unitaries. In panel (a), we present a magnified view of the plot in Fig. 7 when restricted to the range [0.98,1] on the entanglement axis. In panel (b), the same is done for quantum coherence. The vertical axes are again in logarithmic scale for both the panels, (a) and (b). Just one cross-section of the surface in panel (b) is analyzed in panel (c). The chosen cross-section is for $\tilde{C}_g = 1$. The inset and the main plot in panel (c) differ only in the range of the horizontal axis. Please also note that the vertical axis is in the normal scale in panel (c). The analysis in panel (d) is exactly the same as in panel (c), with the roles of entanglement and quantum coherence being reversed. The quantity plotted in the vertical axes is dimensionless, while on the horizontal axes, E_g is in ebits and \tilde{C}_g is in bits. Please see text for more details.

obtain the maximum quantum coherence. Instead of numerically maximizing the entanglement for a unitary, one can also use the canonical decomposition given in [31].

In Fig. 7, we depict E_g and \tilde{C}_g on the base axes, and ν , the relative frequency of the number of unitaries generating the corresponding E_g and \tilde{C}_g , plotted along the vertical axis. Of course, a finite precision is needed for calculating the relative frequencies, and we have a total of 1.6×10^3 squares, with each being of area 2.5×10^{-2} ebits $\times2.5\times10^{-2}$ bits on the entanglement-quantum coherence plane. We generate a total of 2×10^7 two-qubit unitaries, Haar uniformly, and for each square, we plot (on the vertical axis) the relative frequency of the number of unitaries having the ability of generating the numerical values of resources in ebits and bits corresponding to that square.

This depiction describes how the relative frequency increases progressively from ≈ 0 to ≈ 0.7 , as we go along the plane in the direction of increasing entanglement and increasing quantum coherence, and reaches a peak value at the point where entanglement and quantum coherence are both maximal. Note that the vertical axis has a loga-

rithmic scale in the depiction, and this implies that there is a large fraction of unitaries, in the space of two-qubit unitaries, for which both entanglement and quantum coherence generation are near maximal.

In Fig. 8(a), we have focused attention at highentanglement end of Fig. 7. Precisely, we have restricted the entanglement range to [0.98,1], in ebits. Similarly, Fig. 8(b) depicts the same in the high-quantum coherence range, [0.98,1], in bits. We find that there is asymmetry between the entanglement and quantum coherence generations, near their respective maximal values.

In panels (c) and (d) of Fig. 8 we look at both the resources by first fixing the other resource at a fixed value. Precisely, we take the fixed values to be the maximal ones in both cases. In panel (c), the fixed resource is quantum coherence, while in panel (d), it is entanglement. The asymmetric nature between entanglement and quantum coherence generation, as seen in the relative frequencies of Haar random unitaries, that we had mentioned before, is now visible more clearly. We find that the numerically generated red dots in the panels (c) and (d) can be well-described by the beta distribution, suitably scaled and

shifted. But the parameters of the beta distributions that fit the two cases are different. The fitting function therefore has the form,

$$f_B(x) = dB(x; \alpha_B, \beta_B) + h, \tag{34}$$

for $x \in [0,1]$, and $\alpha_B > 0$, $\beta_B > 0$. The explicit form of the beta distribution, $B(x; \alpha_B, \beta_B)$, is given in Appendix B. For Fig. 8(c), the best fit values of the exponents of $f_B(x)$ are as follows:

$$\alpha_B = 3.553 \quad (\pm 0.08559),$$

$$\beta_B = 0.4284 \quad (\pm 0.007544),$$

$$\text{Error} = 8.207 \times 10^{-5}.$$
(35)

The numbers in brackets indicate the respective 95% confidence intervals, and "Error" mentioned is the minimum χ^2 error. The same numbers in Fig. 8(d) are

$$\alpha_B = 11.09 \quad (\pm 1.024),$$

$$\beta_B = 0.03513 \quad (\pm 0.07898),$$

$$Error = 6.443 \times 10^{-4}.$$
(36)

See Appendix B for the values of the other parameters. We have used non-linear least-square fitting to obtain the values of the parameters, their 95% confidence intervals, and the error estimates, for the fitting curves [89].

VI. CONCLUSION

There are two main themes of this manuscript. The first is to find the maximum quantum coherence that can be generated by two-qubit unitary gates from pure incoherent states. And the second is to compare this generation with entanglement generation for the same gate from pure unentangled states, for generic two-qubit unitary gates.

With respect to the first theme, we dealt with the maximum quantum coherence generated by a general twoqubit unitary operator acting on an incoherent pure state of an arbitrary product basis of two qubits. We discussed about the best choice of basis for obtaining the maximum coherence for a fixed unitary, and about the nature of the quantum coherences generated by the unitary when acting on different elements of the basis. The work of Kraus and Cirac [31] had considered the parallel problem for entanglement generation, and had identified a class of two-qubit unitaries, that they called "nonlocal" unitaries. We performed the analysis for the nonlocal unitaries as well as general two-qubit unitaries. We also analyzed the quantum coherence generating capacities of unitaries that can create maximal entanglement, and in parallel, the entanglement generating capacities of maximally quantum coherence generating unitaries.

Finally, we considered the correlation between entanglement and quantum coherence generations for a generic two-qubit unitary, which we generated Haar uniformly by using the Ginibre ensemble. We found that the high entanglement generating unitaries are also typically high quantum coherence generating ones, and conversely, the unitaries that generate high quantum coherence also typically generate high entanglement. However, there is an inherent asymmetry between the entanglement and quantum coherence generations. In particular, we analyzed the profile of the relative frequency of unitaries that can generate maximal entanglement to have the ability to create a given amount of quantum coherence, and found that it can be well-described by the beta distribution. Reversing the roles of entanglement and quantum coherence, one obtains a steeper curve, but still describable by the beta distribution, albeit with a different set of distribution parameters.

ACKNOWLEDGMENTS

We acknowledge computations performed using Armadillo [90, 91], NLOPT [87], (Direct-L [92], ISRES [93], Cobyla [94]) and QIClib [95] on the cluster computing facility of the Harish-Chandra Research Institute, India. We also acknowledge partial support from the Department of Science and Technology, Government of India through the QuEST grant (grant number DST/ICPS/QUST/Theme-3/2019/120).

Appendix A: The constituent quantities of Eq. (31)

The symbols in Eq. (31) have the following meanings.

$$\tilde{\gamma}_{l_1} = \frac{e^{-2i\phi}}{4} \left[e^{i\phi} (r_{l+2} + r_{l+4}) - e^{i\phi} (r_{l+4} - r_{l+2}) \cos \theta + (e^{2i\phi} r_l + r_{l+6}) \sin \theta \right] \\
\times \left[e^{i\phi} (r_{l+4}^* + r_{l+2}^*) - e^{i\phi} (r_{l+4}^* - r_{l+2}^*) \cos \theta + (e^{2i\phi} r_{l+6}^* + r_l^*) \sin \theta \right], \tag{A1}$$

$$\tilde{\delta}_{l_{1}} = \frac{e^{-2i\phi}}{4} \Big[(r_{l+6} - e^{2i\phi}r_{l}) + (r_{l+6} + e^{2i\phi}r_{l}) \cos\theta + e^{i\phi}(r_{l+4} - r_{l+2}) \sin\theta \Big] \\ \times \Big[(e^{2i\phi}r_{l+6}^{*} - r_{l}^{*}) + (e^{2i\phi}r_{l+6}^{*} + r_{l}^{*}) \cos\theta + e^{i\phi}(r_{l+4}^{*} - r_{l+2}^{*}) \sin\theta \Big], \tag{A2}$$

$$\tilde{\gamma}_{l_{2}} = \frac{e^{-2i\phi}}{4} \left[(e^{2i\phi}r_{l} - r_{l+6}) + (e^{2i\phi}r_{l} + r_{l+6})\cos\theta + e^{i\phi}(r_{l+4} - r_{l+2})\sin\theta \right] \\
\times \left[(r_{l}^{*} - e^{2i\phi}r_{l+6}^{*}) + (r_{l}^{*} + e^{2i\phi}r_{l+6}^{*})\cos\theta + e^{i\phi}(r_{l+4}^{*} - r_{l+2}^{*})\sin\theta \right], \tag{A3}$$

$$\tilde{\delta}_{l_{2}} = \frac{e^{-2i\phi}}{4} \left[-e^{i\phi}(r_{l+2} + r_{l+4}) - e^{i\phi}(r_{l+4} - r_{l+2})\cos\theta + (e^{2i\phi}r_{l} + r_{l+6})\sin\theta \right] \\
\times \left[-e^{i\phi}(r_{l+2}^{*} + r_{l+4}^{*}) - e^{i\phi}(r_{l+4}^{*} - r_{l+2}^{*})\cos\theta + (e^{2i\phi}r_{l+6}^{*} + r_{l}^{*})\sin\theta \right]. \tag{A4}$$

Appendix B: Beta distribution and the fitting parameters for panels (c) and (d) of Fig. 8

The beta distribution is a probability density function given by

$$B(x; \alpha_B, \beta_B) = \frac{\Gamma(\alpha_B + \beta_B)}{\Gamma(\alpha_B)\Gamma(\beta_B)} (x - x_0)^{\alpha_B - 1} [1 - (x - x_0)]^{\beta_B - 1},$$
(B1)

for $x \in [0, 1]$, and $\alpha_B > 0$, $\beta_B > 0$. x_0 is a real number. For panel (c) of Fig. 8, the best fit values of the parameters of $f_B(x)$ and their respective 95% confidence intervals, within the nonlinear least-square fit method,

are

$$\begin{split} \alpha_B &= 3.553 \quad (\pm 0.08559), \\ \beta_B &= 0.4284 \quad (\pm 0.007544), \\ d &= 0.002755 \quad (\pm 3.004 \times 10^{-5}), \\ x_0 &= 5.138 \times 10^{-5} \quad (\pm 4.267 \times 10^{-6}), \\ h &= 8.125 \times 10^{-5} \quad (\pm 1.952 \times 10^{-5}). \end{split} \tag{B2}$$

The values of the same parameters in Fig. 8(d) are

$$\alpha_B = 11.09 \quad (\pm 1.024),$$

$$\beta_B = 0.03513 \quad (\pm 0.07898),$$

$$d = 0.1440 \quad (\pm 0.3187),$$

$$x_0 = 0.007000 \quad (\pm 0.0009043),$$

$$h = 0.0002362 \quad (\pm 0.0001067).$$
(B3)

- [1] M. B. Plenio and S. Virmani, An Introduction to entanglement measures, Quant. Inf. Comput. 7, 1 (2007).
- [2] R. Horodecki, P. Horodecki, M. Horodecki and K. Horodecki, Quantum entanglement, Rev. Mod. Phys. 81, 865 (2009).
- [3] O. Gühne and G. Tóth, Entanglement detection, Physics Reports 474, 1 (2009).
- [4] S. Das, T. Chanda, M. Lewenstein, A. Sanpera, A. Sen(De) and U. Sen, The separability versus entanglement problem, in Quantum Information, edited by D. Bruß and G. Leuchs (Wiley, Weinheim, 2019), chapter 8.
- [5] C. H. Bennett, G. Brassard, C. Crépeau, R. Jozsa, A. Peres and W. K. Wootters, Teleporting an unknown quantum state via dual classical and Einstein-Podolsky-Rosen channels, Phys. Rev. Lett. 70, 1895 (1993).
- [6] S. Pirandola, J. Eisert, C. Weedbrook, A. Furusawa and S. L. Braunstein, Advances in quantum teleportation, Nat. Photonics 9, 641 (2015).
- [7] T. Liu, The Applications and Challenges of Quantum Teleportation, J. Phys.: Conf. Ser. 1634, 012089 (2020).
- [8] N. Gisin, G. Ribordy, W. Tittel, H. Zbinden, Quantum Cryptography, Rev. Mod. Phys. 74, 145 (2002).
- [9] S. Pirandola, U. L. Andersen, L. Banchi, M. Berta, D. Bunandar, R. Colbeck, D. Englund, T. Gehring, C. Lupo, C. Ottaviani, J. Pereira, M. Razavi, J. S. Shaari, M. Tomamichel, V. C. Usenko, G. Vallone, P. Villoresi and P. Wallden, Advances in Quantum Cryptography, Adv. Opt. Photon. 12, 1012 (2020).

- [10] C. Portmann and R. Renner, Security in Quantum Cryptography, arXiv:2102.00021.
- [11] C. H. Bennett, S. J. Wiesner, Communication via oneand two-particle operators on Einstein-Podolsky-Rosen states, Phys. Rev. Lett. 69, 2881 (1992).
- [12] Y. Guo, B. H. Liu, C. F. Li and G. C. Guo, Advances in quantum dense coding, Advanced Quantum Technologies, 2, 1900011, (2019).
- [13] J. Åberg, Quantifying Superposition, arXiv:quant-ph/0612146.
- [14] T. Baumgratz, M. Cramer and M. B. Plenio, Quantifying Coherence, Phys Rev Lett, 113, 140401 (2014).
- [15] A. Winter and D. Yang, Operational Resource Theory of Coherence, Phys. Rev. Lett. 116, 120404 (2016).
- [16] A. Streltsov, G. Adesso and M. B. Plenio, Quantum Coherence as a Resource, Rev. Mod. Phys. 89, 041003 (2017).
- [17] T. Theurer, N. Killoran, D. Egloff and M. B. Plenio, Resource Theory of Superposition, Phys. Rev. Lett. 119, 230401 (2017); S. Das, C. Mukhopadhyay, S. S. Roy, S. Bhattacharya, A. Sen(De) and U. Sen Wave-particle duality employing quantum coherence in superposition with non-orthogonal pointers, J. Phys. A: Math. Theor. 53, 115301 (2020).
- [18] C. Srivastava, S. Das and U. Sen, Resource theory of quantum coherence with probabilistically nondistinguishable pointers and corresponding wave-particle duality, Phys. Rev. A 103, 022417 (2021).

- [19] I. Banerjee, K. Sen, C. Srivastava and U. Sen, Quantum coherence with incomplete set of pointers and corresponding wave-particle duality, arXiv:2108.05849.
- [20] D. P. Pires, I. A. Silva, E. R. deAzevedo, D. O. Soares-Pinto and J. G. Filgueiras, Coherence orders, decoherence and quantum metrology, Phys. Rev. A 98, 032101 (2018).
- [21] A. Castellini, R. Lo Franco, L. Lami, A. Winter, G. Adesso and G. Compagno, *Indistinguishability-enabled coherence for quantum metrology*, Phys. Rev. A 100, 012308 (2019).
- [22] C. Zhang, T. R. Bromley, Y.-F. Huang, H. Cao, W.-M. Lv, B.-H. Liu, C.- F. Li, G.-C. Guo, M. Cianciaruso and G. Adesso, Demonstrating quantum coherence and metrology that is resilient to transversal noise, Phys. Rev. Lett. 123, 180504 (2019).
- [23] M. Hillery, Coherence as a resource in decision problems: The Deutsch-Jozsa algorithm and a variation, Phys. Rev. A 93, 012111 (2016).
- [24] N. Anand and A. K. Pati, Coherence and Entanglement Monogamy in the Discrete Analogue of Analog Grover Search, arXiv:1611.04542.
- [25] H.-L. Shi, S.-Y. Liu, X.- H. Wang, W.-L. Yang, Z.-Y. Yang and H. Fan, Coherence depletion in the Grover quantum search algorithm, Phys. Rev. A 95, 032307 (2017).
- [26] Y.-C. Liu, J. Shang and X. Zhang, Coherence Depletion in Quantum Algorithms, Entropy 21, 260 (2019).
- [27] Shubhalakshmi S and U. Sen, Noncommutative coherence and quantum phase estimation algorithm, arXiv:2004.01419.
- [28] C. Xiong and J. Wu, Geometric coherence and quantum state discrimination, J. Phys. A: Math. Theor. 51, 414005 (2018).
- [29] S. Kim, L. Li, A. Kumar, C. Xiong, S. Das, U. Sen, A. K. Pati and J. Wu, *Unambiguous quantum state discrimination with quantum coherence*, arXiv:1807.04542.
- [30] P. Zanardi, Entanglement of Quantum Evolutions, Phys. Rev. A 63, 040304 (2001).
- [31] B. Kraus and J. I. Cirac, Optimal Creation of Entanglement Using a Two-Qubit Gate, Phys. Rev. A 63, 062309 (2001).
- [32] F. Verstraete, K. Audenaert and B. D. Moor, Maximally entangled mixed states of two qubits, Phys. Rev. A 64, 012316 (2001).
- [33] K. Życzkowski, P. Horodecki, M. Horodecki and R. Horodecki, *Dynamics of quantum entanglement*, Phys. Rev. A 65, 012101 (2002).
- [34] M. S. Leifer, L. Henderson and N. Linden, Optimal entanglement generation from quantum operations, Phys. Rev. A 67, 012306 (2003).
- [35] X. Wang, B. C. Sanders and D. W. Berry, Entangling power and operator entanglement in qudit systems, Phys. Rev. A 67, 042323 (2003).
- [36] P. J.Dodd and J. J.Halliwell, Disentanglement and decoherence by open system dynamics, Phys. Rev. A 69, 052105 (2004).
- [37] A. R. R. Carvalho, F. Mintert and A. Buchleitner, Decoherence and multipartite entanglement, Phys. Rev. Lett. 93, 230501 (2004).
- [38] W. Dür and H.-J. Briegel, Stability of macroscopic entanglement under decoherence, Phys. Rev. Lett. 92, 180403 (2004).

- [39] M. P. Almeida, F. De Melo, M. Hor-Meyll, A. Salles, S. P. Walborn, P. H. Souto Ribeiro and L. Davidovich, *Environment-induced sudden death of entanglement*, Science 316, 579 (2007).
- [40] A. R. R. Carvalho, M. Busse, O. Brodier, C. Viviescas and A. Buchleitner, *Optimal dynamical characterization* of entanglement, Phys. Rev. Lett. 98, 190501 (2007).
- [41] H. Bao-Lin and D. Yao-Min, Entanglement Capacity of Two-Qubit Unitary Operator with the Help of Auxiliary System, Commun. Theor. Phys. 47, 1029 (2007).
- [42] T. Konrad, F. de Melo, M. Tiersch, C. Kasztelan, A. Aragão and A. Buchleitner, Evolution equation for quantum entanglement, Nature Physics 4, 99 (2008).
- [43] S. M. Cohen, All maximally entangling unitary operators, Phys. Rev. A 84, 052308 (2011).
- [44] F. Fröwis, Kind of entanglement that speeds up quantum evolution, Phys. Rev. A 85, 052127 (2012).
- [45] A. Chefles, Entangling capacity and distinguishability of two-qubit unitary operators, Phys. Rev. A 72, 042332 (2005).
- [46] S. Ishizaka and T. Hiroshima, Maximally entangled mixed states under nonlocal unitary operations in two qubits, Phys. Rev. A 62, 022310 (2000).
- [47] J. Batle, A. R. Plastino, M. Casas and A. Plastino, On the distribution of entanglement changes produced by unitary operations, Phys. Lett. A 307, 253 (2003).
- [48] M. Ye, D. Sun, Y. Zhang and G. Guo, Entanglementchanging power of two-qubit unitary operations, Phys. Rev. A 70, 022326 (2004).
- [49] X. Wang and P. Zanardi, Quantum entanglement of unitary operators on bipartite systems Phys. Rev. A 66, 044303 (2002).
- [50] J. K. Asbóth, J. Calsamiglia and H. Ritsch, Computable Measure of Nonclassicality for Light, Phys. Rev. Lett. 94, 173602 (2005).
- [51] Y. Yao, X. Xiao, L. Ge and C. P. Sun, Quantum coherence in multipartite systems, Phys. Rev. A 92, 022112 (2015).
- [52] N. Killoran, F. E. S. Steinhoff and M. B. Plenio, Converting non-classicality into entanglement, arXiv:1505.07393.
- [53] A. Streltsov, U. Singh, H. S. Dhar, M. N. Bera and G. Adesso Measuring Quantum Coherence with Entanglement, Phys. Rev. Lett. 115, 020403 (2015).
- [54] Z. Xi, Y. Li and H. Fan Quantum coherence and correlations in quantum system, Sci. Rep. 5, 10922 (2015).
- [55] A. Streltsov, E. Chitambar, S. Rana, M. N. Bera, A. Winter and M. Lewenstein, Entanglement and Coherence in Quantum State Merging, Phys. Rev. Lett. 116, 240405 (2016).
- [56] N. Killoran, F. E. S. Steinhoff and M. B. Plenio Converting Nonclassicality into Entanglement, Phys. Rev. Lett. 116, 080402 (2016).
- [57] X. Qi, T. Gao and F. Yan Measuring Coherence with Entanglement Concurrence, J. Phys. A: Math. Theor. 50, 285301 (2017).
- [58] S. Chin, Coherence number as a discrete quantum resource, Phys. Rev. A 96, 042336 (2017).
- [59] H. Zhu, Z. Ma, Z. Cao, S. Fei and V. Vedral, Operational one-to-one mapping between coherence and entanglement measures, Phys. Rev. A 96, 032316 (2017).
- [60] H. Zhu, M. Hayashi and L. Chen Axiomatic and operational connections between the l1-norm of coherence and negativity, Phys. Rev. A. 97, 022342 (2018).

- [61] A. Mekala and U. Sen, All entangled states are quantum coherent with locally distinguishable pointers, arXiv:2008.11148 [quant-ph].
- [62] K. Bu, A. Kumar and J. Wu Bell-type inequality in quantum coherence theory as an entanglement witness, arXiv:1603.06322.
- [63] L. Qiu, Z. Liu and F. Pan, Tripartite Bell-type inequalities for measures of quantum coherence and skew information, arXiv:1610.07237.
- [64] D. Mondal, T. Pramanik and A. K. Pati, Nonlocal advantage of quantum coherence, Phys. Rev. A 95, 010301 (2017).
- [65] T. Chanda and S. Bhattacharya Delineating incoherent non-Markovian dynamics using quantum coherence, Annals of Physics 366, 1 (2016).
- [66] S. Bhattacharya, S. Banerjee and A. K. Pati, Evolution of coherence and non-classicality under global environmental interaction, Quantum Inf. Process. 17, 236 (2018).
- [67] Z. Huang and H. Situ, Optimal Protection of Quantum Coherence in Noisy Environment, International Journal of Theoretical Physics 56, 503 (2017).
- [68] B. Cakmak, M. Pezzutto, M. Paternostro and Ö. E. Müstecaplioğlu, Non-Markovianity, coherence and system-environment correlations in a long-range collision model, Phys. Rev. A 96, 022109 (2017).
- [69] C. Mukhopadhyay, S. Bhattacharya, A. Misra and A. K. Pati, Dynamics and thermodynamics of a central spin immersed in a spin bath, Phys. Rev. A 96, 052125 (2017).
- [70] A. Mortezapour, M. Ahmadi Borji and R. Lo Franco, Non-Markovianity and coherence of a moving qubit inside a leaky cavity, Open Systems and Information Dynamics 24, 1740006 (2017).
- [71] J. Ma, B. Yadin, D. Girolami, V. Vedral and M. Gu, Converting Coherence to Quantum Correlations, Phys. Rev. Lett. 116, 160407 (2016).
- [72] J. M. Matera, D. Egloff, N. Killoran and M. B. Plenio, Coherent control of quantum sys- tems as a resource theory, Quantum Science and Technology 1, 01LT01 (2016).
- [73] Y. Guo and S. Goswami, Discordlike correlation of bipartite coherence, Phys. Rev. A. 95, 062340 (2017).
- [74] D. W. Berry and B. C. Sanders, Relation between classical communication capacity and entanglement capability for two-qubit unitary operations, Phys. Rev. A 68, 032312 (2003).
- [75] A. Misra, U. Singh, S. Bhattacharya and A. K. Pati, Energy cost of creating quantum coherence, Phys. Rev. A 93, 052335 (2016).
- [76] Y. Yao, X. Xiao, L. Ge and C. P. Sun, Quantum coherence in multipartite systems, Phys. Rev. A 92, 022112 (2015).
- [77] L. Zhang, Z. Ma, Z. Chen and S. M. Fei, Coherence generating power of unitary transformations via probabilistic average, Quantum Information Processing 17, 186 (2018).
- [78] G. Styliaris, L. C. Venuti and P. Zanardi, Coherencegenerating power of quantum dephasing processes, Phys.

- Rev. A 97, 032304 (2018).
- [79] C. H. Bennett, D. DiVincenzo, J. A. Smolin and W. K. Wootters, Mixed State Entanglement and Quantum Error Correction, Phys. Rev. A 54, 3824 (1996).
- [80] E. M. Rains, Rigorous treatment of distillable entanglement, Phys. Rev. A 60, 173 (1999).
- [81] P. M. Hayden, M. Horodecki and B. M. Terhal, The asymptotic entanglement cost of preparing a quantum state, J. Phys. A: Math. Gen. 34, 6891 (2001).
- [82] C. H. Bennett, H. J. Bernstein, S. Popescu and B. Schumacher, Concentrating Partial Entanglement by Local Operations, Phys. Rev. A 53, 2046 (1996).
- [83] J. Walgate and L. Hardy, Nonlocality, Asymmetry, and Distinguishing Bipartite States, Phys. Rev. Lett. 89, 147901 (2002).
- [84] N. Khaneja and S. Glaser, Cartan Decomposition of SU(2ⁿ), Constructive Controllability of Spin systems and Universal Quantum Computing, arXiv:quantph/0010100.
- [85] S. Hill and W. K. Wootters, Entanglement of a Pair of Quantum Bits, Phys. Rev. Lett. 78, 5022 (1997).
- [86] W. K. Wootters, Entanglement of Formation of an Arbitrary State of Two Qubits, Phys. Rev. Lett. 80, 2245 (1998).
- [87] S. G. Johnson, The NLopt nonlinear-optimization package, http://github.com/stevengj/nlopt.
- [88] M. Ozols, How to generate a random unitary matrix (2009). Available at http://home.lu.lv/~sd20008/ papers/essays/Random%20unitary%20%5Bpaper%5D. pdf.
- [89] D. M. Bates and D. G. Watts, Nonlinear Regression Analysis and Its Applications (Wiley, New York, 1988);
 W. H. Press, S. A. Teukolsky, W. T. Vetterling and B. P. Flannery, Numerical Recipes: The Art of Scientific Computing (Cambridge University Press, Cambridge, 2007);
 A. Sehrawat, C. Srivastava and U. Sen, Dynamical phase transitions in the fully connected quantum Ising model: Time period and critical time, Phys. Rev. B 104, 085105 (2021), Appendix E.
- [90] C. Sanderson and R. Curtin, Armadillo: a template-based C++ library for linear algebra, Journal of Open Source Software 1, 26 (2016).
- [91] C. Sanderson and R. Curtin, Lecture Notes in Computer Science (LNCS) 10931, 422 (2018).
- [92] J. M. Gablonsky and C. T. Kelley, A locally-biased form of the DIRECT algorithm, J. Global Optimization, 21,27 (2001).
- [93] T. P. Runarsson and X. Yao, Search biases in constrained evolutionary optimization, IEEE Trans. on Systems, Man, and Cybernetics Part C: Applications and Reviews, 35, 233 (2005).
- [94] M. J. D. Powell, Direct search algorithms for optimization calculations, Acta Numerica 7, 336 (1998).
- [95] T. Chanda, QIClib, https://titaschanda.github.io/ QIClib.